**Cell Reports Medicine, Volume *4***

## Supplemental information

# Two pan-SARS-CoV-2 nanobodies and their multivalent derivatives effectively prevent Omicron infections in mice

**Honghui Liu, Lili Wu, Bo Liu, Ke Xu, Wenwen Lei, Jianguo Deng, Xiaoyu Rong, Pei Du, Lebing Wang, Dongbin Wang, Xiaolong Zhang, Chao Su, Yuhai Bi, Hua Chen, William J. Liu, Jianxun Qi, Qingwei Cui, Shuhui Qi, Ruiwen Fan, Jingkun Jiang, Guizhen Wu, George F. Gao, and Qihui Wang**

Supplementary Materials for

# Two pan-SARS-CoV-2 nanobodies and their multivalent derivatives effectively prevent Omicron infections in mice

**Honghui Liu[1,11], Lili Wu[1,11], Bo Liu[1,2,11], Ke Xu[3,11], Wenwen Lei[3,11], Jianguo Deng[4,11], Xiaoyu Rong[1,5], Pei Du[1], Lebing Wang[4], Dongbin Wang[4], Xiaolong Zhang[6], Chao Su[1,7], Yuhai Bi[1], Hua Chen[6], William J. Liu[3], Jianxun Qi[1,8], Qingwei Cui[9], Shuhui Qi[2], Ruiwen Fan[2,*], Jingkun Jiang[4,*], Guizhen Wu[3,*], George F. Gao[1,10,*], Qihui Wang[1,5,8,12,*]**

*Corresponding author. Email: ruiwenfan@163.com (R. F.); jiangjk@tsinghua.edu.cn (J. J.); wugz@ivdc.chinacdc.cn (G. W.); gaof@im.ac.cn (G. F. G.); wangqihui@im.ac.cn (Q. W.).

## This PDF file includes

**Table S1. Data collection and refinement statistics of nanobody R14 or S43 in complex with SARS-CoV-2 RBD.** Related to Fig. 6.

| | nanobody R14/ RBD | nanobody S43/ RBD |
|---|---|---|
| **Data collection** | | |
| Space group | P3221 | C2221 |
| Cell dimension | | |
| a, b, c (Å) | 92.45, 92.45, 218.745 | 102.279, 138.886, 122.72, |
| α, β, λ (°) | 90, 90, 120 | 90, 90, 90 |
| Resolution (Å) | 2.50-46.22 | 2.70-50 (2.7-2.8)[a] |
| Unique reflections | | 24629 |
| $R_{merge}$ | | 0.176(0.796) |
| $R_{pim}$ | | 0.994(0.872) |
| $I / \sigma I$ | | 16.4(3.0) |
| Completeness (%) | | 100(100) |
| Redundancy | | 13.1(12.2) |
| **Refinement** | | |
| Resolution (Å) | 2.500-46.225 | 2.686-49.205 |
| No. reflections | 35975 | 24510 |
| $R_{work}/R_{free}$ | 0.2006/0.2395 | 0.2038/0.2293 |
| No. atoms | | |
| Protein | 5064 | 5111 |
| Ligands | 62 | 104 |
| Water | 200 | 89 |
| Average B-factors (Å$^2$) | | |
| Protein | 47.70 | 46.01 |
| Ligands | 101.79 | 82.15 |
| Water | 42.83 | 37.81 |
| RMSD | | |
| Bond lengths (Å) | 0.003 | 0.003 |
| Bond angles (°) | 0.640 | 0.603 |
| Ramachandran plot [e] | | |
| Favored (%) | 97.04% | 97.67 |
| Allowed (%) | 2.96% | 2.33 |
| Outliers (%) | 0.00% | 0.00 |

The highest resolution shell is shown in parentheses.

**Table S2. Nanobody R14 in complex with SARS-CoV-2 RBD**. Related to Fig. 6.

| **SARS-CoV-2 RBD** | **nanobody R14** |
|---|---|
| Y351 | Y104 (2) |
| R403 | D118 (10, 2) |
| K417 | G115 (1) |
| V445 | D30 (1) |
| G446 | T28 (5), L29 (7), D30 (14, 1) |
| G447 | L29 (2) |
| Y449 | L29 (6), D30 (6, 1), Y31 (17, 2), P100 (2), A101 (8), Y103 (4), Y108 (6) |
| N450 | Y103 (2) |
| L452 | T102 (1), Y103 (4) |
| Y453 | G116 (2) |
| L455 | P113 (2), G115 (2), G116 (4) |
| F456 | P113 (2) |
| T470 | Y104 (9) |
| T478 | D62 (1) |
| V483 | Y109 (3), Q111 (2), |
| F486 | G47 (6), V48 (7), S49 (6), C50 (2), S59 (8), Y60 (19), A61 (16) |
| C488 | Q111 (1) |
| Y489 | Q111 (15), C112 (3), P113 (6) |
| F490 | T102 (2), Y104 (9), Y109 (24), Q111 (14, 3) |
| L492 | T102 (5, 1), Y104 (2), Q111 (1) |
| Q493 | T99 (3), P100 (8,1), A101 (1), T102 (13, 1), P113 (1) |
| S494 | P100 (3), A101 (4), T102 (15, 1), Y103 (6, 1) |
| Y495 | P100 (3), D118 (1) |
| G496 | L29 (3), P100 (3) |
| Q498 | T28 (8,1), L29 (12), Y119 (1) |
| N501 | Y119 (1, 1) |
| Y505 | D118 (17, 1), Y119 (3) |
| Total | 377, 17 |

The numbers in parentheses of nanobody R14 residues represent the numbers of vdw contacts the indicated residues conferred. The numbers behind comma suggest numbers of potential H-bonds between the pairs of residues. vdw contact was analyzed at a cutoff of 4.5 Å and H-bonds at a cut off of 3.5 Å.

**Table S3. Nanobody S43 in complex with SARS-CoV-2 RBD**. Related to Fig. 6.

| **SARS-CoV-2 RBD** | **nanobody S43** |
|---|---|
| Y369 | Y107 (23, 1) |
| F374 | T108 (2) |
| S375 | T108 (2), C109 (1), G110 (5, 1), W111 (1), T112 (10,1), D113 (1) |
| T376 | T108 (3), T112 (9, 1), D113 (10,1) |
| F377 | Y106 (2), Y107 (17, 1), T108 (12, 1) |
| K378 | V104 (3), Y105 (5), Y106 (3), Y107 (1), D113 (8, 1) |
| C379 | G103 (1), V104 (4), Y105 (14, 2) |
| Y380 | D100 (1), S102 (4), G103 (4), V104 (13) |
| G381 | G103 (1), Y105 (4) |
| V382 | Y105 (12) |
| S383 | Y105 (7) |
| P384 | Y105 (6), Y106 (4), Y107 (4) |
| G404 | W111 (5), T112 (2) |
| D405 | W111 (3) |
| V407 | T112 (8) |
| R408 | E98 (13, 1), T112 (3,1), F114 (2), G115 (2) |
| P412 | Y101 (1), S102 (4) |
| G413 | Y101 (4) |
| Q414 | E98 (4, 1), P99 (4, 1), Y101 (1) |
| D427 | S102 (1) |
| V503 | W111 (8) |
| G504 | W111 (3) |
| Y508 | W111 (7), T112 (4) |
| Total | 276,14 |

The numbers in parentheses of nanobody S43 residues represent the numbers of vdw contacts the indicated residues conferred. The numbers behind comma suggest numbers of potential H-bonds between the pairs of residues. vdw contact was analyzed at a cutoff of 4.5 Å and H-bonds at a cut off of 3.5 Å.

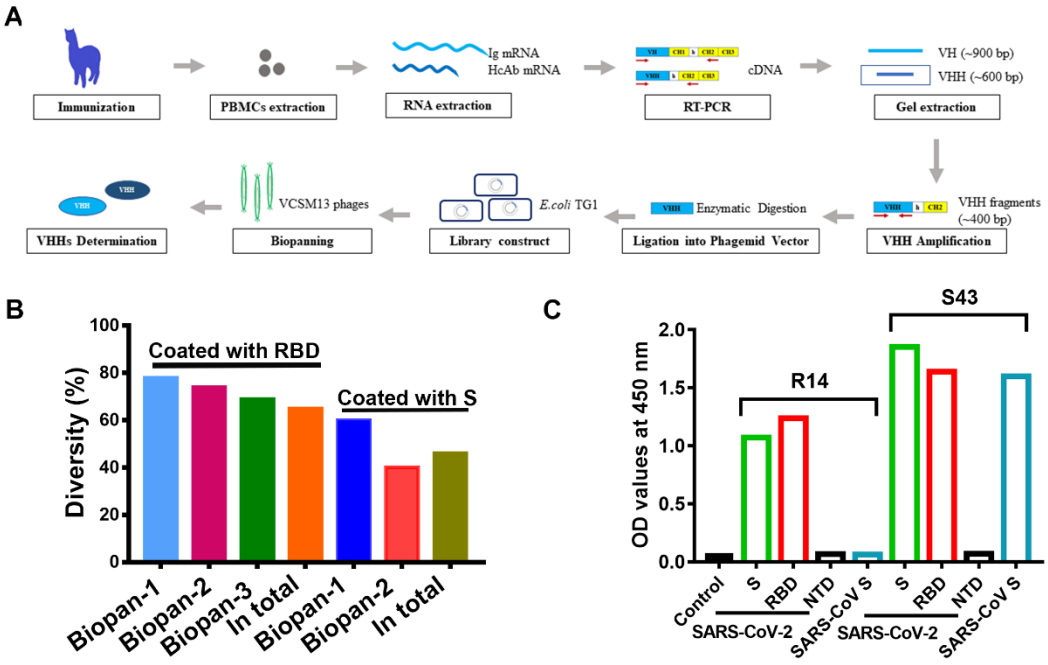


**Figure S1. The generation and determination of nanobodies.** Related to Fig. 1. (A) Overview of the nanobody generation process. (B) Diversity of amino acid sequences in biopanning steps. (C) ELISA binding to different antigens from SARS-CoV-2 and SARS-CoV by R14 or S43, respectively.

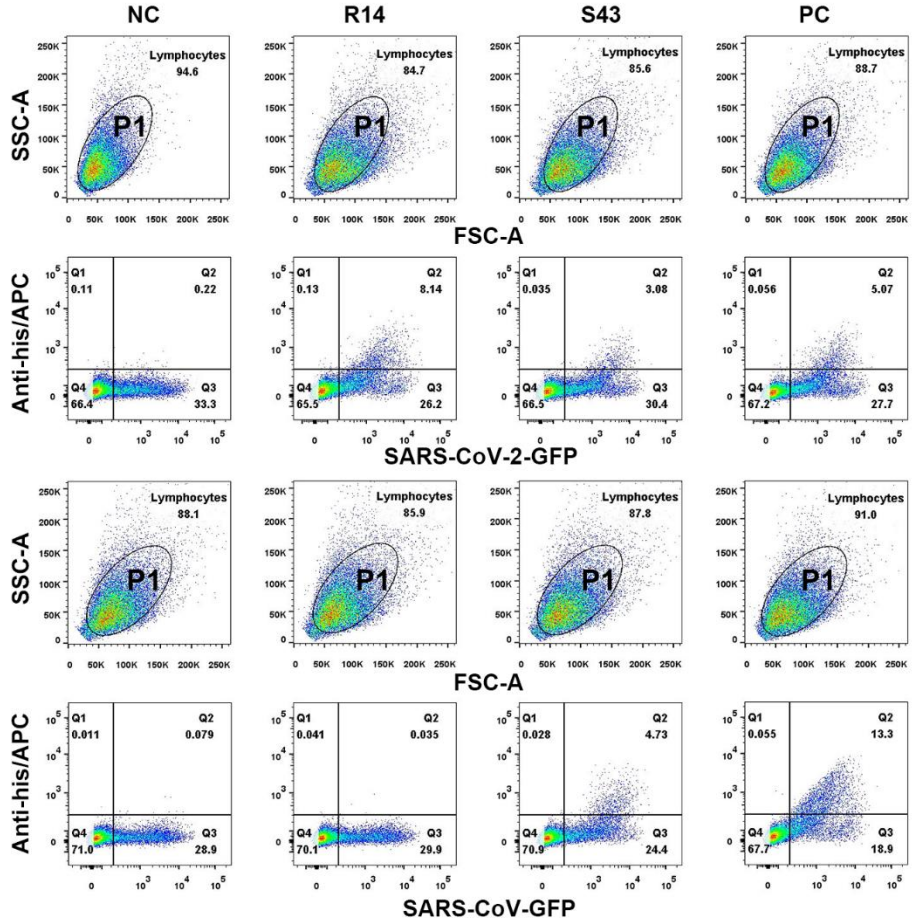


**Figure S2. Gating strategy and binding determination between nanobodies and SARS-CoV-2 or SARS-CoV by a FACS-based assay.** Related to Fig. 1. GFP-fused SARS-CoV-2 or SARS-CoV spike (S) protein was transiently expressed on the surface of BHK-21 cells, and strained with his-tagged nanobodies. 'NC' presents negative control that was performed without nanobody protein. 'PC' presents positive control that was performed with one nanobody that can bind to both SARS-CoV-2 and SARS-CoV S protein. Then flow cytometry were conducted using BD FACSCanto. Cells were gated based on the FSC-A and SSC-A (P1).

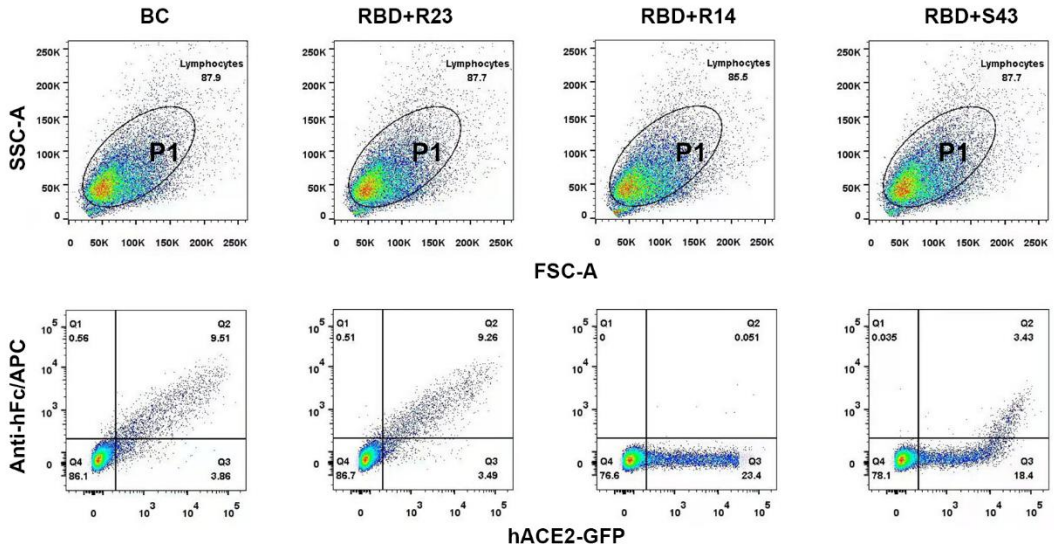


**Figure S3. Gating strategy and blocking evaluation.** Related to Fig. 1. FACS-based assay showing that R14 and S43 can block SARS-CoV-2 RBD binding to human ACE2 (hACE2). hACE2-GFP fusion protein was transiently expressed on the surface of BHK-21 cells and stained with SARS-CoV-2 RBD protein, which are pre-incubated with His-tagged R14 or S43. Experiments were performed twice, and one representative data is displayed. 'BC' presents the blank control that was performed without nanobody. R23, as an irrelevant nanobody, presents the negative control. Then flow cytometry were conducted using BD FACSCanto. Cells were gated based on the FSC-A and SSC-A (P1).

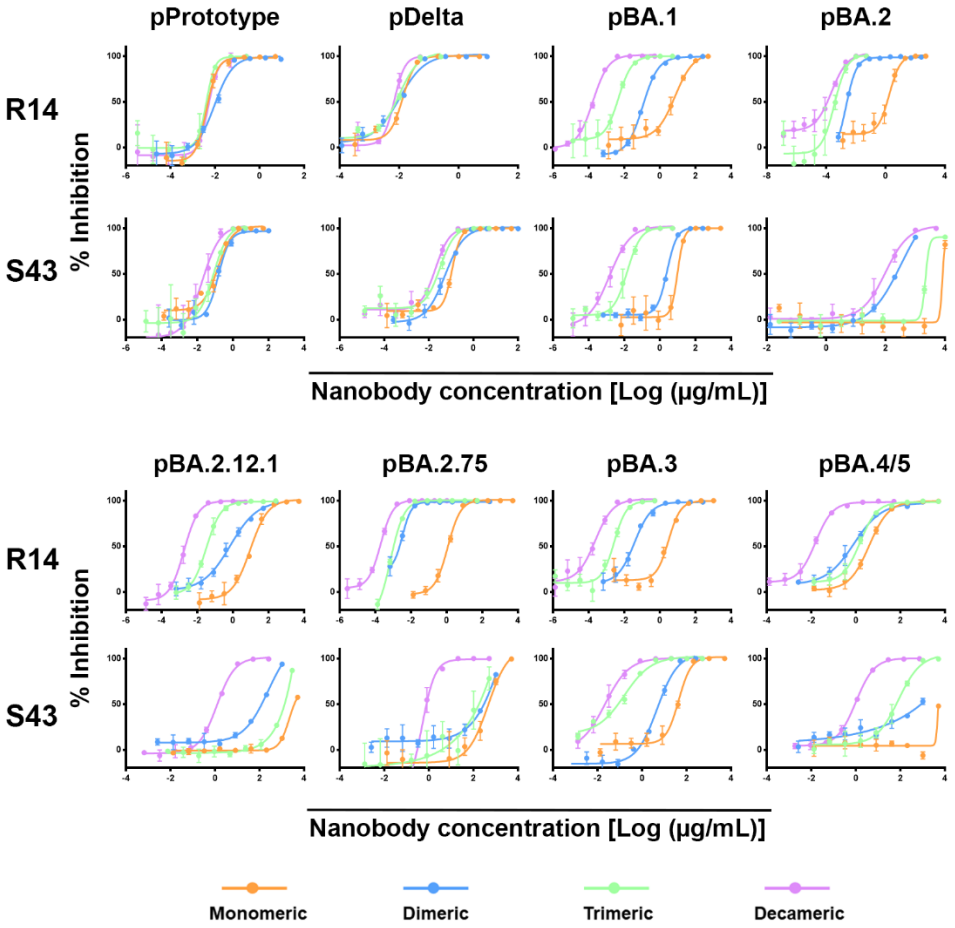


**Figure S4. Neutralization curves of nanobodies and their multivalent derivatives against pseudotyped SARS-CoV-2 variants or sub-variants in Vero cells.** Related to Fig. 4. Experiments were independently repeated three times with similar results, and one representative curve is displayed. The orange, blue, green and violet lines indicated the neutralization curves of the monomeric, dimeric, trimeric and decameric antibodies, respectively.

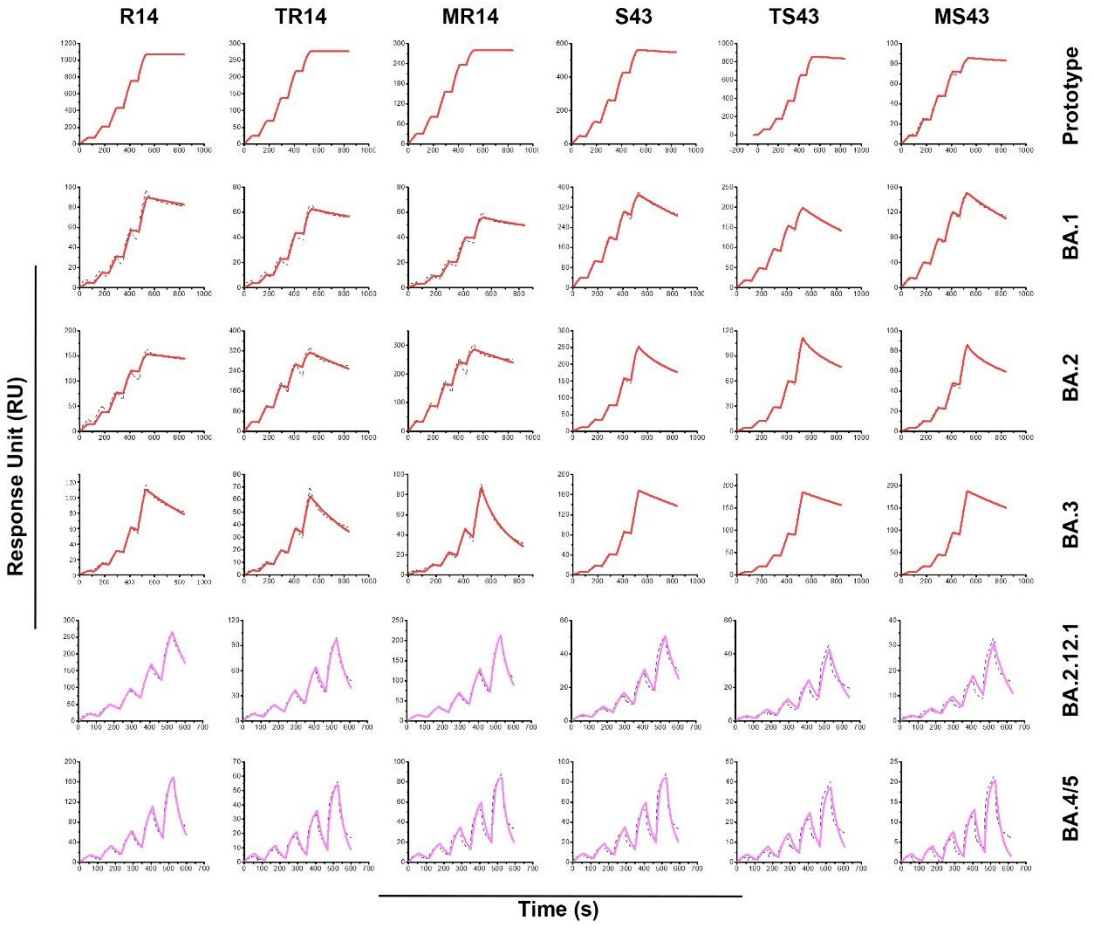


| | | R14 | TR14 | MR14 | S43 | TS43 | MS43 |
|---|---|---|---|---|---|---|---|
| Prototype (with 300s) | $k_a$ (1/Ms) | 3.6±0.9e+5 | 4.2±0.5e+5 | 5.6±1.1e+5 | 4.0±0.1e+5 | 6.9±0.3e+5 | 1.1±0.1e+6 |
| | $k_d$ (1/s) | - | - | - | 1.2±0.5e-4 | 1.3±0.2e-4 | 1.1±0.1e-4 |
| | $K_D$ (nM) | | | | 0.3±0.1 | 0.2±0.04 | 0.1±0.01 |
| | $Chi^2$ | 8 | 1.3 | 0.8 | 2.5 | 5.1 | 0.9 |
| | Rmax | 1233.4 | 295.2 | 287.3 | 613.4 | 889.1 | 88.2 |
| BA.1 (with 300s) | $k_a$ (1/Ms) | 1.2±0.2e+5 | 8.7±4.8e+5 | 8.6±2.6e+5 | 3.1±0.1e+5 | 8.0±2.0e+5 | 9.4±2.6e+5 |
| | $k_d$ (1/s) | 4.3±2.2e-4 | 6.8±2.0e-4 | 6.3±1.1e-4 | 7.5±0.7e-4 | 1.1±0.03e-3 | 1.8±1.1e-3 |
| | $K_D$ (nM) | 3.2±1.1 | 0.88±0.35 | 0.77±0.26 | 2.5±0.3 | 1.5±0.5 | 2.4±2.2 |
| | $Chi^2$ | 1.1 | 4.2 | 2.6 | 19.3 | 3.2 | 2.8 |
| | Rmax | 127.9 | 63.9 | 56.8 | 395.7 | 218.5 | 163.2 |
| BA.2 (with 300s) | $k_a$ (1/Ms) | 4.3±0.4e+5 | 5.2±1.3e+5 | 6.4±2.1e+5 | 3.1±4.5e+5 | 1.5±0.2e+5 | 1.3±1.9e+6 |
| | $k_d$ (1/s) | 2.4±0.8e-4 | 3.9±3.1e-4 | 2.9±2.4e-4 | 1.6±1.5e-3 | 6.6±0.3e-4 | 3.4±2.3e-3 |
| | $K_D$ (nM) | 0.57±0.13 | 0.70±0.38 | 0.44±0.36 | 2.7±0.8 | 4.6±0.8 | 5.6±3.4 |
| | $Chi^2$ | 29.7 | 80.8 | 91.2 | 4.3 | 0.6 | 1 |
| | Rmax | 166.6 | 330.4 | 295 | 270.8 | 124.6 | 92.9 |
| BA.3 (with 300s) | $k_a$ (1/Ms) | 7.2±1.8e+4 | 7.3±4.3e+4 | 8.9±7.8e+8 | 1.9±0.1e+4 | 3.6±2.1e+4 | 2.3±0.7e+4 |
| | $k_d$ (1/s) | 1.4±0.3e-3 | 3.5±1.4e-3 | 1.5±1.0e+1 | 7.2±0.4e-4 | 1.2±0.5e-3 | 7.6±1.0-4 |
| | $K_D$ (nM) | 20.2±1.6 | 24.9±13.2 | 20.5±11.5 | 37.5±3.5 | 35.1±7.7 | 36.7±1.9 |
| | $Chi^2$ | 3.4 | 3.9 | 3.3 | 0.8 | 0.4 | 0.6 |
| | Rmax | 278.2 | 112.2 | 146.1 | 859.1 | 1174 | 675 |
| BA.2.12.1 (with 80s) | $k_a$ (1/Ms) | 2.1±0.1e+5 | 5.0±0.5e+5 | 7.2±7.2e+5 | 4.1±2.5e+5 | 3.5±3.2e+5 | 1.8±1.1e+5 |
| | $k_d$ (1/s) | 6.7±1.3e-3 | 1.9±0.4e-2 | 4.5±2.9e-2 | 2.7±2.2e-2 | 2.6±2.3e-2 | 1.4±0.8e-2 |
| | $K_D$ (nM) | 32.6±4.5 | 38.2±3.7 | 39.0±8.8 | 71.5±11.5 | 75.9±7.0 | 79.3±5.3 |
| | $Chi^2$ | 30.8 | 8.7 | 60.5 | 6.2 | 8.2 | 4.9 |
| | Rmax | 445.7 | 151.2 | 326.3 | 102.3 | 115.5 | 76 |
| BA.4/5 (with 80s) | $k_a$ (1/Ms) | 1.3±0.2e+6 | 2.7±3.3e+6 | 1.1±1.0e+7 | 4.0±0.5e+5 | 3.8±0.5e+5 | 3.8±0.3e+5 |
| | $k_d$ (1/s) | 5.8±1.0e-2 | 1.5±1.6e-1 | 4.9±3.8e-1 | 4.0±0.3e-2 | 1.9±0.1e-2 | 8.6±0.5e-2 |
| | $K_D$ (nM) | 43.3±0.03 | 61.4±10.3 | 50.3±10.3 | 100±7.9 | 51.8±8.0 | 69.8±14.5 |
| | $Chi^2$ | 26.1 | 7.7 | 27.3 | 8 | 9.2 | 3.7 |
| | Rmax | 270.5 | 98.6 | 126.8 | 95.3 | 67.3 | 42.7 |

**Figure S5. The binding kinetics of antibodies to RBDs of SARS-CoV-2 and Omicron sub-variants using a BIAcore 8K system in single-cycle mode.** Related to Fig. 4. The raw curves are shown as black

dotted lines. The fitting curves with the dissociation time of 300s and 80s using 1:1 Langmuir binding model are shown as red and violet solid lines, respectively. The values of $k_a$, $k_d$, $K_D$, and the parameters ($Chi^2$ value and $R_{max}$) are listed as the mean ± s.d. of three independent experiments. "-" represents no detectable dissociation from the RBD.

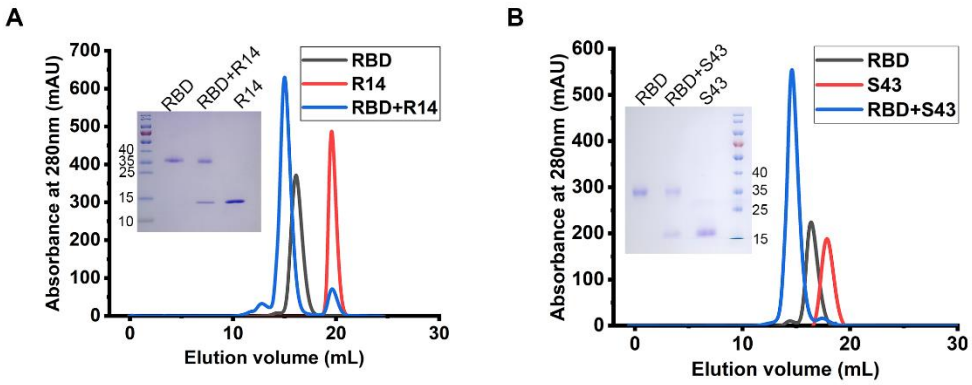


**Figure S6. Gel filtration profile of SARS-CoV-2 RBD and R14 (A) or S43 (B).** Related to Fig. 6. The SARS-CoV-2 RBD, R14 or S43 proteins elute as single monomer peaks in the gel filtration curves. The SARS-CoV-2 RBD/R14 complex or SARS-CoV-2 RBD/S43 complex displays a shifted complex peak. All the samples were assessed by SDS-PAGE.

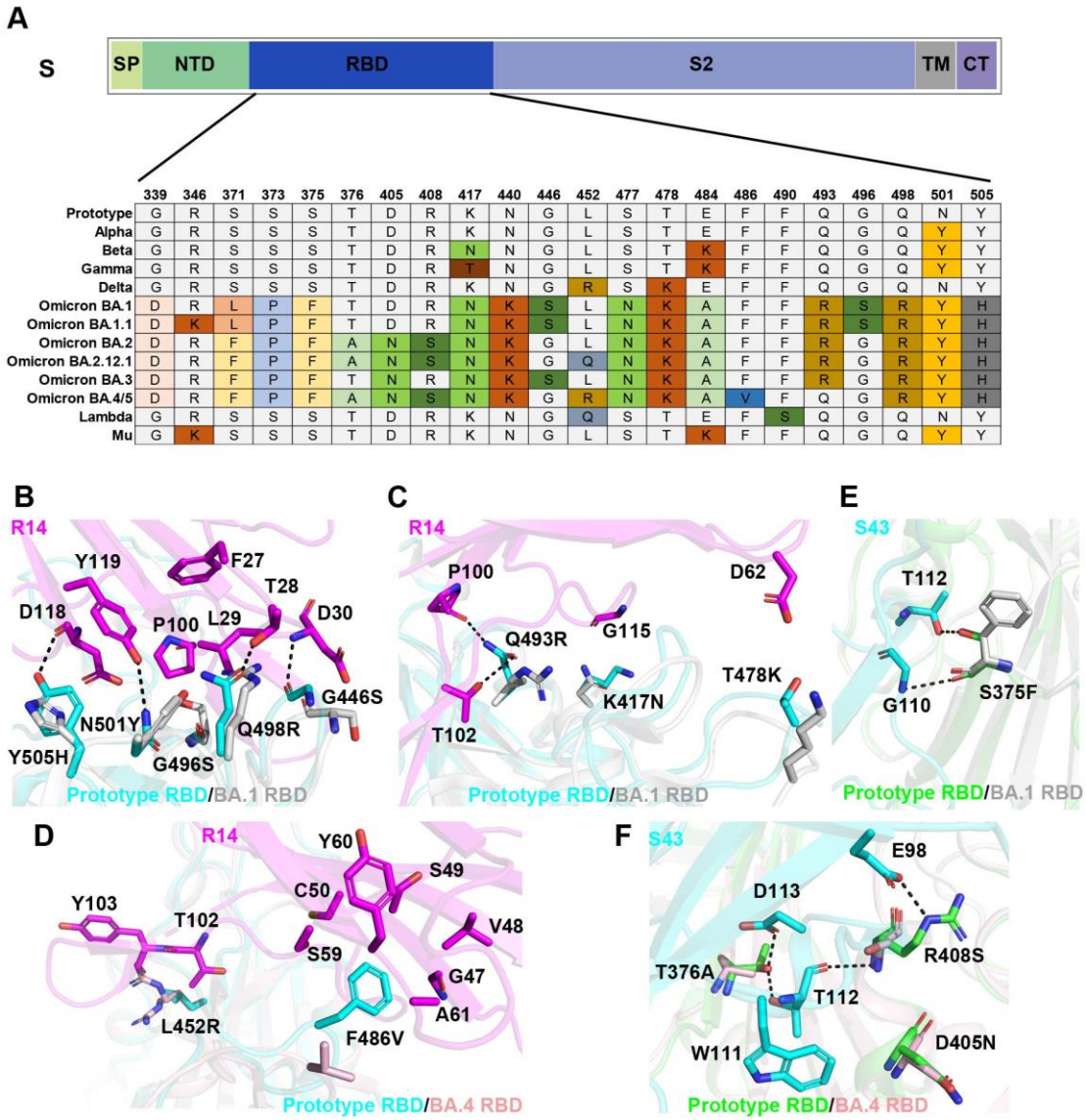


**Figure S7. The amino acid substitutions on RBDs of VOCs and VOIs, and structural details of key mutations in Omicron sub-variants interacting with R14 or S43.** Related to Fig. 6. (A) The schematic diagram shows the SARS-CoV-2 S protein. The amino acid substitutions on RBDs of five VOCs and two VOIs are displayed. (B-F) Binding face between RBD and R14 (B-D) or S43 (E-F). BA.1 RBD (7X1M) and BA.4 RBD (7ZXU) were used to align with Prototype RBD binding with R14 or S43. All structures were shown in cartoon with the key residues in stick. H-bonds were shown as dotted lines with a cutoff of 3.5 Å.